

Communication

Ionic Exchange of Metal-Organic Frameworks to Access Single Nickel Sites for Efficient Electroreduction of CO₂

Changming Zhao, xinyao dai, Tao Yao, Wenxing Chen, Xiaoqian Wang, Jing Wang, Jian Yang, Shiqiang Wei, Yuen Wu, and Yadong Li

J. Am. Chem. Soc., **Just Accepted Manuscript** • Publication Date (Web): 08 Jun 2017

Downloaded from <http://pubs.acs.org> on June 8, 2017

Just Accepted

“Just Accepted” manuscripts have been peer-reviewed and accepted for publication. They are posted online prior to technical editing, formatting for publication and author proofing. The American Chemical Society provides “Just Accepted” as a free service to the research community to expedite the dissemination of scientific material as soon as possible after acceptance. “Just Accepted” manuscripts appear in full in PDF format accompanied by an HTML abstract. “Just Accepted” manuscripts have been fully peer reviewed, but should not be considered the official version of record. They are accessible to all readers and citable by the Digital Object Identifier (DOI®). “Just Accepted” is an optional service offered to authors. Therefore, the “Just Accepted” Web site may not include all articles that will be published in the journal. After a manuscript is technically edited and formatted, it will be removed from the “Just Accepted” Web site and published as an ASAP article. Note that technical editing may introduce minor changes to the manuscript text and/or graphics which could affect content, and all legal disclaimers and ethical guidelines that apply to the journal pertain. ACS cannot be held responsible for errors or consequences arising from the use of information contained in these “Just Accepted” manuscripts.



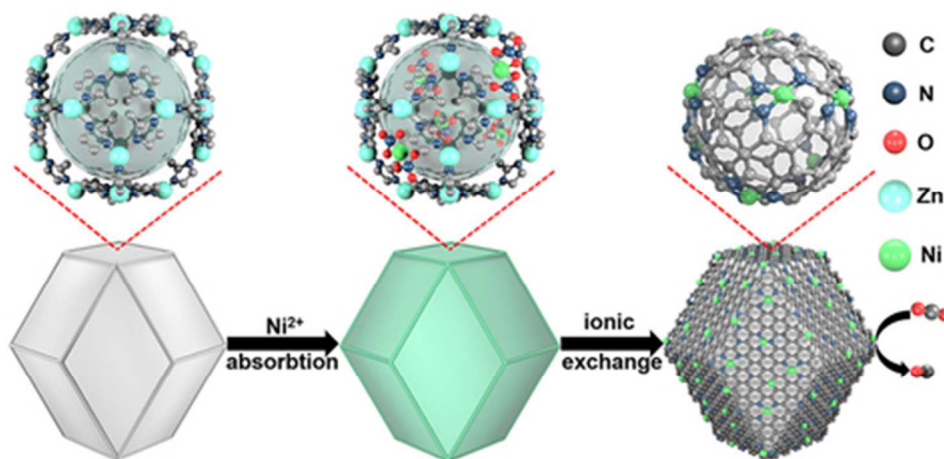


Table of content

40x19mm (300 x 300 DPI)

Ionic Exchange of Metal-Organic Frameworks to Access Single Nickel Sites for Efficient Electroreduction of CO₂

Changming Zhao,[†] Xinyao Dai,[†] Tao Yao,^{*,§} Wenxing Chen[‡], Xiaoqian Wang,[†] Jing Wang,[†] Jian Yang,[†] Shiqiang Wei,[§] Yuen Wu,^{*,†} and Yadong Li^{*,‡}

[†] Department of Chemistry, iChEM (Collaborative Innovation Center of Chemistry for Energy Materials), University of Science and Technology of China, Hefei 230026, China

[‡] Department of Chemistry and Collaborative Innovation Center for Nanomaterial Science and Engineering, Tsinghua University, Beijing 100084, China

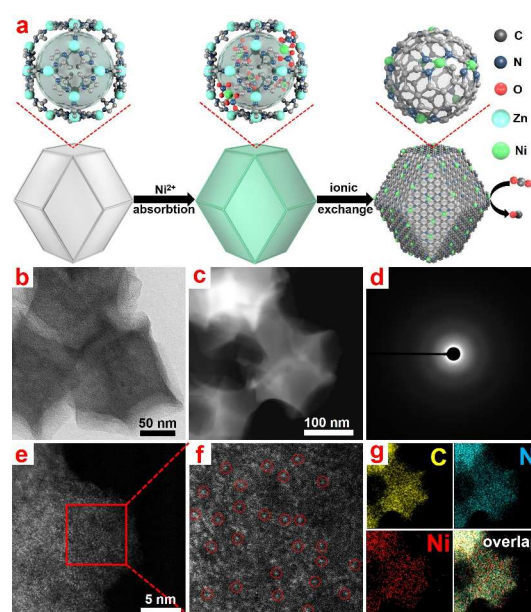
[§] Hefei National Laboratory for Physical Sciences at the Microscale, University of Science and Technology of China, Hefei, Anhui Province 230026, (China)

Supporting Information Placeholder

ABSTRACT: Single atom catalysts often exhibit unexpected catalytic activity for many important chemical reactions due to their unique electronic and geometric structures with respect to bulk counterparts. Herein, we adopt metal-organic frameworks to assist the preparation of single Ni sites catalyst for efficient electroreduction of CO₂. The synthesis is based on the ionic exchange between Zn nodes and adsorbed Ni ions within the cavities of MOFs. This single atoms catalyst gained an excellent turnover frequency (5273 h⁻¹) for electroreduction of CO₂, with a faradaic efficiency for CO production over 71.9% and current density of 10.48 mA cm⁻² at 0.89 V overpotential. Our findings present some guidelines for the rational design and accurate modulation over nanostructured catalysts at atomic scale.

Due to the increase concentration of atmospheric CO₂ and limited reservoir of fossil fuels, there is urgent need for designing robust and efficient catalysts to convert greenhouse CO₂ into valuable chemicals¹⁻⁴. Electroreduction of CO₂ into value-added products is an effective approach to remit the environmental and energy issues, during which the electricity can be generated from renewable energy sources such as, solar, wind and tidal power. However, achieving the electroreduction of CO₂ usually needs to overcome some bottlenecks including large overpotential for electron transfer from catalyst to CO₂ and multiple distribution of products derived from the competitive side reactions such as hydrogen evolution reaction (HER)^{5,6}. As a result, searching for the active and selective catalysts is of paramount crucial to make practical CO₂ electroreduction a reality. Over the past decades, researchers have evaluated lots of materials as electrodes for CO₂ electroreduction, such as metal, transition metal oxide, transition metal chalcogenides, carbon-based material and metal-organic framework.^{5,7} The intrinsic reaction mechanism of CO₂ electroreduction involves complicated pathways occurring at solid-liquid-gas three-phase boundaries^{8,9}. Thus, rational design of the geometric structure of catalyst to exposed the reactive sites as more as possible is important to facilitate the mass and electron

transfer at the interface¹⁰. Moreover, the modulation of local structure such as metal-ligands interplay, bonds length,



coordination number, and so on over the reactive sites also play a vital role in the efficient activation of CO₂ and selective desorption of products.

Figure 1. (a) Scheme of the formation of Ni SAs-N/C. (b) TEM and (c) HAADF-STEM images of Ni SA/N-C. (d) Corresponding SAED pattern of an individual rhombododecahedron. (e, f) Magnified HAADF-STEM images of Ni SAs/N-C, and the Ni single atoms were marked with red circle. (h) The corresponding EDS mapping reveals the homogeneous distribution of Ni and N on the carbon support.

Owing to high ratio of low-coordinated metal atoms and technically uniform structure, the single-atom catalysts have shown its great potential as ideal catalysts for some chemical transformation¹¹⁻¹³. However, not only the universality of synthetic methodology for single-atom catalysts but also the

accurate control over the microstructures still needs improvement due to the high mobility and diffusivity of sub-nano species^{15,16}. In this rapidly developed research topic, the single atoms catalysts have been demonstrated as highly active catalysts for CO oxidation reactions^{11,17}, hydrogenation reactions¹⁶, oxidation reactions¹⁸ and so on¹⁹. Nevertheless, the electroreduction of CO₂ catalyzed by the single atoms materials has been seldomly studied.

Assembled from the Zn²⁺ nodes and 2-methylimidazole (MeIm), ZIF-8 [Zn(MeIm)₂] is a class of Metal-organic frameworks (MOFs) with high crystallinity and ultrafine porosity¹⁹⁻²¹. In this work, we have developed a ZIFs-assisted strategy to generate Ni single atoms distributing in nitrogen-doped porous carbon (Ni SAs/N-C) for active CO₂ reduction¹⁵. The turnover frequency (TOF) normalized to single Ni sites reached a value of 5273 h⁻¹ and the selectivity (based on the faradaic efficiency) for CO production is over 71.9% at 0.89 V overpotential. A mechanism illustrating the formation process of Ni SAs/N-C is summarized in Figure 1.

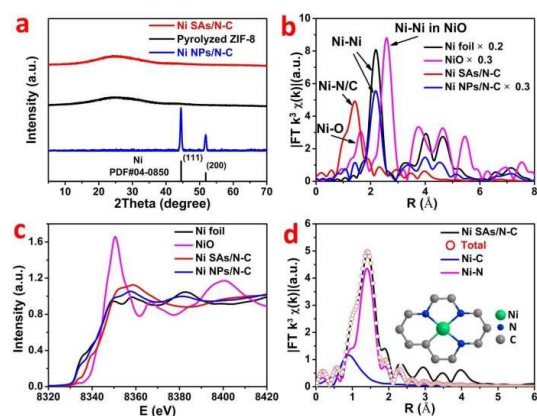


Figure 2. (a) XRD patterns of Ni SAs/N-C, Ni NPs/N-C and pyrolyzed ZIF-8. (b) Ni K-edge XANES spectra and (c) the k^3 -weighted $\chi(k)$ -function of the EXAFS spectra. (d) The corresponding EXAFS fitting curves for Ni SAs/N-C. Inset is the proposed Ni-N₃ architectures.

The initial ZIF-8 was first synthesized in methanol at room temperature according to the typical method²¹, which exhibited uniform rhombododecahedral shape and narrow size distribution with an average size of 200 nm (Figure S1). As shown by X-ray powder diffraction (XRD) patterns in Figure S2, the as-prepared sample showed a typical crystal patterns as ZIF-8. Subsequently, the ZIF-8 was homogeneously dispersed in n-hexane, followed with the injection of Ni(NO₃)₂ aqueous solution. Through a double solvents approach, the Ni precursor could be confined within the pores of ZIF-8 even the small hexagonal window size was only 3.3 Å^{21,24}. Afterward, this mixture was pyrolyzed at 1000 °C under the protection of Ar flow, during which the organic linkers transform into N-doped carbon skeleton. The pyrolysis of ZIF-8 was clearly tracked by thermogravimetric analysis (TGA, Figure S3). The typical weight loss at about 600 °C was attributed to linker decomposition of ZIF-8 such as CN fragments. When the temperature was elevated over 900 °C, the weight loss may resulted from the release of Zn species. That is, the Zn nodes with low boiling point of 907 °C would evaporate at such high temperature, leaving the N-rich defects¹⁵. These sites would be easily occupied by the neighbor ionic Ni atoms and provided a protective fence

to avoid the aggregation. Hence, the isolated Ni atoms was stabilized by N coordination and further reduced by the surrounding carbon. Verified by the Brunauer-Emmett-Teller (BET) measurement (Figure S4), the Ni SAs/N-C inherited the high surface area and abundant porosity of ZIF-8, which is conducive to the electrolyte diffusion and mass transfer. To further demonstrate the Ni SAs/N-C exhibited remarkably large active surface, endowing excellent CO₂ adsorption capacity, we carry out the CO₂ adsorption isotherms (Figure S5) measurement. By increasing the quantity of adsorbed Ni(NO₃)₂, a color evolution from white to green was observed and the Ni NPs would form during the pyrolysis due to the insufficient anchoring sites (Figure S6, S7). The formation of large nanoparticles in the sample of Ni NPs/N-C could be also verified by the external magnet. (Figure S6 d, h).

The TEM image (Figure 1b and Figure S8) and high-angle annular dark-field scanning transmission electron microscope (HAADF-STEM) image (Figure 1c) both reveal that the as-prepared Ni SAs/N-C structure retains the initial rhombododecahedral shape and size distribution of the starting polyhedrons. The ring-like selected area electron diffraction (SAED) pattern taken from an individual rhombododecahedron demonstrated its poor crystallinity (Figure 1d). Aberration corrected HAADF-STEM image of Ni SAs/N-C showed that the Ni atoms dominantly presented the atomic dispersion (Figure 1e and 1f). The isolated heavier Ni SAs could be discerned in the carbon support because of a different Z-contrast between Ni, N and C. Energy dispersive X-ray spectroscopy (EDS) analysis in a scanning transmission electron microscope (STEM) revealed that Ni and N homogeneously dispersed on the whole structure (Figure 1g). The actual loading of Ni is 1.53 %, which was measured by inductively coupled plasma optical emission spectroscopy (ICP-OES). One can see there was no characteristic peaks of Ni crystals emerged in the XRD pattern of Ni SAs/N-C (Figure 2a), demonstrating the poor crystallinity. With increasing the content of adsorbed Ni, a set of well-defined face-centered cubic Ni peaks emerged at 44.3 ° and 51.7 ° under similar pyrolysis conditions, indicating the formation of nanoparticles.

The X-ray photoelectron spectroscopy (XPS) was further used to characterize the valence state and composition evolution during the synthesis (Figure S9, S10). For Ni SAs/N-C, the binding energy of the Ni 2p_{3/2} peak was 855.12 eV and thus higher than that reported for Ni⁰ (852.5-853.0 eV) and lower than Ni²⁺ (853.7 eV), which revealed the ionic Ni^{δ+} (0 < δ < 2) nature in the Ni SAs/N-C. This results coincided well with the reported results that the valence of Ni species usually situated between the Ni (0) and Ni (II)^{12,25}. Furthermore, more detailed structural informations can be obtained from the X-ray absorption fine structure (XAFS). The Fourier transforms (FT) k^3 -weighted $\chi(k)$ -function of the extended X-ray absorption fine structure (EXAFS) for Ni SAs/N-C exhibited dominant Ni-N coordination with a peak at 1.42 Å (Figure 2b). Together with the deficiency of Ni-Ni path, the atomic dispersion of single Ni sites could be corroborated. By contrast, the main peak for Ni NPs/N-C was closer to 2.18 Å, belonging to the Ni-Ni coordination. As shown in the X-ray absorption near-edge structure (XANES) spectra of Ni SAs/N-C (Figure 2c), the intensity of white line located between the Ni foil and NiO, which clear told the

unique electronic structure of $\text{Ni}^{\delta+}$ ($0 < \delta < 2$). This observation also agrees well with the aforementioned XPS results. According to the fitting results, the proposed local structure of Ni SAs/N-C with three N coordination was presented as the inset in Figure 3d.

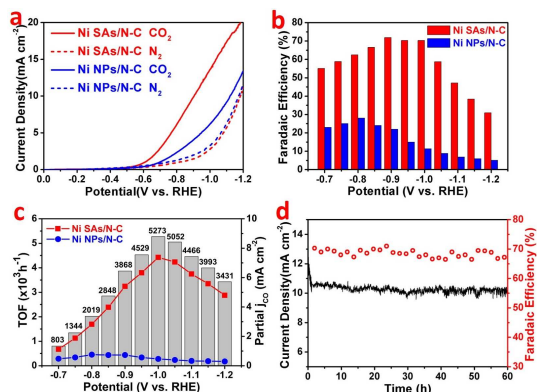
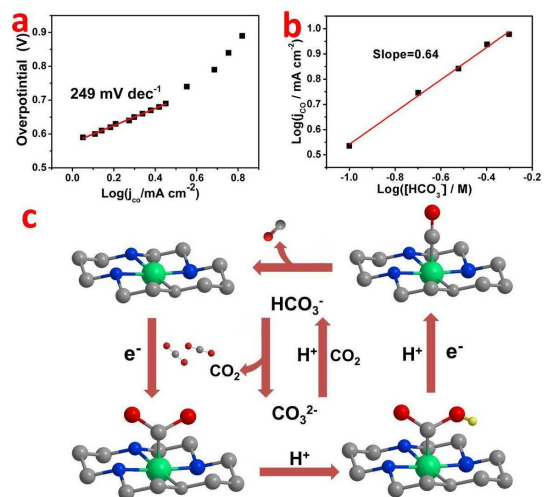


Figure 3. (a) LSV curves in the N_2 -saturated (dotted line) or CO_2 -saturated (solid line) 0.5 M KHCO_3 electrolyte with a 10 mV s^{-1} scan rate. (b) FEs of CO and (c) Partial CO current density (based on geometric surface area) plots and TOFs of the Ni SAs/N-C and Ni NPs/N-C at different applied potentials. (d) Stability of the Ni SAs/N-C at the potential of -1.0 V versus RHE for Ni SAs/N-C during 60 h.

The electroreduction of CO_2 was performed in a two-compartment gas-tight cell, which was separated by a Nafion-115 proton exchange membrane to prevent the oxidation of as-generated products. The cathodic compartment was continuously purged with CO_2 with a constant flow rate of 10 ml min^{-1} and vented directly into the gas-sampling loop ($20 \mu\text{L}$) for the periodic quantification of the gas-phase products by a gas chromatograph (GC). Liquid products formed in the CO_2 reduction were not detected by ^1H nuclear magnetic resonance (NMR) spectroscopy after reduction processes (Figure S11). The comparison of the CO_2 reduction activity based on Ni SAs/N-C and Ni NPs/N-C is summarized in Figure 3. According to the results of linear sweep voltammetry (LSV), the Ni SAs/N-C exhibited an onset potential of -0.57 V versus RHE (reversible hydrogen electrode; all potentials are with reference to RHE), which was much more positive relative to Ni NPs/N-C (Figure 3a). This result was both confirmed in the N_2 -saturated 0.5 M NaClO_4 solution and CO_2 -saturated 0.5 M KHCO_3 to exclude the affect of HCO_3^- (Figure S12). In addition, the current density catalyzed by Ni SAs/N-C reached a high value of 10.48 mA cm^{-2} at -1.0 V , which was roughly 3 times larger than that of Ni NPs/N-C (Figure S13). The analysis by ^1H NMR and GC suggested the primary products catalyzed by Ni SAs/N-C and Ni NPs/N-C were CO and H_2 . The Faradaic Efficiencies (FEs) of CO strictly depends on the working potential. At the potential of -0.9 V , the Ni SAs/N-C attained a maximum FEs of 71.9%, which was over 3 times than that of Ni NPs/N-C. As is shown in Figure 3c, the partial CO current density of the Ni SAs/N-C showed 30 times larger than that of the Ni NPs/N-C in the applied potentials of -0.95 V to -1.2 V . What's more, at -1.0 V , the Ni SAs/N-C attained a maximum of partial CO current density of 7.37 mA cm^{-2} and a TOFs of 5273 h^{-1} . To the best of our knowledge, this

catalytic behavior outperformed most of the reported catalysts (Table S2).

The electrocatalytic reduction of CO_2 on pyrolyzed ZIF-8 was performed to investigate the crucial role of Ni centers in the same condition. Both current density and FEs for CO production decrease obviously, when catalyzed by this Ni-free material (Figure S14). Moreover, if the commercial Ni foam was utilized as the cathodic material, a sluggish current density was found and the main product was detected to be H_2 . This result evidenced the downsizing of bulk Ni would largely vary the surface structure of catalysts and thus affect a relative different catalytic performance. Interestingly, the current density of Ni foam was even lower in the CO_2 -



saturated electrolyte than in N_2 -saturated electrolyte (Figure S15). This confirmed the surface of Ni foam may be poisoned by the generated CO, which further restricted the HER⁶. In contrast, the Ni SAs/N-C exhibited a long-term stability of 60 h operation, during which no obvious decay in Faradaic efficiency and current density was detected (Figure 3d).

Figure 4. (a) Tafel plots of the partial CO current density for Ni SAs/N-C at different applied potentials. (b) Partial CO current density of Ni SAs/N-C vs. potassium bicarbonate concentration at constant potential. (c) Proposed reaction paths for CO_2 electroreduction of Ni SAs/N-C.

The Ni SAs/N-C shows a clearly improved CO_2 reduction performances may be attributed to the increased surface active sites, lower adsorption energy of CO over single Ni sites and improved electronic conductivity²⁷. The result in Nyquist plots revealed that the Ni SAs/N-C has lower interfacial charge-transfer resistance (R_{CT}) than Ni NPs/N-C (Figure S17), hence ensuring faster electron transfer from electrodes to CO_2 and easier formation of $\text{CO}_2^{\cdot-}$ radical anion intermediate. As shown in Figure 4a, the Tafel slope of 249 mV dec^{-1} reached by Ni SAs/N-C was different with the reported bulk and nanometer-sized materials^{28,29}, which indicated a different mechanism for the reduction of carbon dioxide². In addition, a plot of $\log(j_{\text{CO}})$ vs. $\log([\text{HCO}_3^-])$ shows a slope of 0.64 in Figure 4b, indicating the HCO_3^- concentration could apparently influence the efficiency of CO_2 electroreduction. The HCO_3^- may not only simply act as a proton donor in the reaction solution, but also increase the concentration of CO_2 via rapid equilibrium with bicarbonate³⁰. Since the Ni SAs showed abundant low-coordinated sites on surface, the strong bonding with the $\text{CO}_2^{\cdot-}$ may account for the excellent performance for CO_2

electroreduction (Figure 4c). Unfortunately, the Ni SAs/N-C also exhibited a competitive activity towards HER^{12,25}, which significantly depress the high Faradaic efficiency for CO production. The structural modification over the reactive Ni sites at atomic scale for the purpose of simultaneously achieving high activity and selectivity for CO₂ electroreduction are still demanded in future study.

In summary, Ni SAs/N-C has been successfully synthesized by ionic exchange of Zn nodes and adsorbed Ni salts. Compared with Ni NPs and Ni foam, Ni SAs are capable of selectively reducing CO₂ with excellent current density and FEs. Our findings shed light to the rational design at molecular reactive sites for various practical applications.

ASSOCIATED CONTENT

Supporting Information

Detailed experimental procedures; SEM and TEM images; BET data, TGA data; XPS data. This material is available free of charge via the Internet at <http://pubs.acs.org>.

AUTHOR INFORMATION

Corresponding Author

yaot@ustc.edu.cn;

yuenwu@ustc.edu.cn;

ydli@mail.tsinghua.edu.cn

Author Contributions

Changming Zhao and Xinyao Dai contributed equally to this work.

Notes

The authors declare no competing financial interests.

ACKNOWLEDGMENT

This work was supported by China Ministry of Science and Technology under Contract of 2016YFA (0202801), and the National Natural Science Foundation of China (21522107, 21671180, 21521091, 21390393, U1463202). This work made use of the resources and finance support of National Synchrotron Radiation Laboratory in Beijing and Shanghai. We thank the Photoemission Endstations (BL10B) in National Synchrotron Radiation Laboratory (NSRL) for help in characterizations.

REFERENCES

- (1) Costentin, C.; Drouet, S.; Robert, M.; Savéant, J.-M. *Science* **2012**, *338*, 90-94.
- (2) Lin, S.; Diercks, C. S.; Zhang, Y.-B.; Kornienko, N.; Nichols, E. M.; Zhao, Y.; Paris, A. R.; Kim, D.; Yang, P.; Yaghi, O. M. *Science* **2015**, *349*, 1208-1213.
- (3) Gao, S.; Lin, Y.; Jiao, X.; Sun, Y.; Luo, Q.; Zhang, W.; Li, D.; Yang, J.; Xie, Y. *Nature* **2016**, *529*, 68-71.
- (4) Asadi, M.; Kim, K.; Liu, C.; Addepalli, A. V.; Abbasi, P.; Yasaei, P.; Phillips, P.; Behranginia, A.; Cerrato, J. M.; Haasch, R. *Science* **2016**, *353*, 467-470.
- (5) Zhu, D. D.; Liu, J. L.; Qiao, S. Z. *Adv. Mater.* **2016**, *28*, 3423-3452.
- (6) Feng, X.; Jiang, K.; Fan, S.; & Kanan, M. W. *J. Am. Chem. Soc.* **2015**, *137*, 4606-4609.
- (7) Albo, J.; Vallejo, D.; Beobide, G.; Castillo, O.; Castaño, P.; & Irabien, A. *ChemSusChem*, **2017**, *10*, 1100-1109.
- (8) He J, Hu B, Zhao Y. *Adv. Funct. Mater.* **2016**, *26*, 5998-6004.
- (9) Lu, Z., Xu, W., Ma, J., Li, Y., Sun, X., & Jiang, L. *Adv. Mater.* **2016**, *28*, 7155-7161.
- (10) Zitolo, A.; Goellner, V.; Armel, V.; Sougrati, M.-T.; Mineva, T.; Stievano, L.; Fonda, E.; Jaouen, F. *Nature Mater.* **2015**, *14*, 937-942.
- (11) Qiao, B.; Wang, A.; Yang, X.; Allard, L. F.; Jiang, Z.; Cui, Y.; Liu, J.; Li, J.; Zhang, T. *Nature Chem.* **2011**, *3*, 634-641.
- (12) Qiu, H. J.; Ito, Y.; Cong, W.; Tan, Y.; Liu, P.; Hirata, A.; Fujita, T.; Tang, Z.; Chen, M. *Angew. Chem., Int. Ed.* **2015**, *127*, 14237-14241.
- (13) Jones, J.; Xiong, H.; DeLaRiva, A. T.; Peterson, E. J.; Pham, H.; Challa, S. R.; Qi, G.; Oh, S.; Wiebenga, M. H.; Hernández, X. I. P. *Science* **2016**, *353*, 150-154.
- (14) Liu, P.; Zhao, Y.; Qin, R.; Mo, S.; Chen, G.; Gu, L.; Chevrier, D. M.; Zhang, P.; Guo, Q.; Zang, D. *Science* **2016**, *352*, 797-800.
- (15) Yin, P.; Yao, T.; Wu, Y.; Zheng, L.; Lin, Y.; Liu, W.; Ju, H.; Zhu, J.; Hong, X.; Deng, Z. *Angew. Chem., Int. Ed.* **2016**, *55*, 10800-10805.
- (16) Zhang, B.; Asakura, H.; Zhang, J.; Zhang, J.; De, S.; Yan, N. *Angew. Chem., Int. Ed.* **2016**, *55*, 8319-8323.
- (17) Guan, H.; Lin, J.; Qiao, B.; Yang, X.; Li, L.; Miao, S.; Liu, J.; Wang, A.; Wang, X.; Zhang, T. *Angew. Chem., Int. Ed.* **2016**, *128*, 2870-2874.
- (18) Deng, D.; Chen, X.; Yu, L.; Wu, X.; Liu, Q.; Liu, Y.; Yang, H.; Tian, H.; Hu, Y.; Du, P. *Sci. Adv.* **2015**, *1*, e1500462.
- (19) Guo, X.; Fang, G.; Li, G.; Ma, H.; Fan, H.; Yu, L.; Ma, C.; Wu, X.; Deng, D.; Wei, M. *Science* **2014**, *344*, 616-619.
- (20) Park, K. S.; Ni, Z.; Côté, A. P.; Choi, J. Y.; Huang, R.; Uribe-Romo, F. J.; Chae, H. K.; O'Keeffe, M.; Yaghi, O. M. *Proc. Natl. Acad. Sci.* **2006**, *103*, 10186.
- (21) Huang, X. C.; Lin, Y. Y.; Zhang, J. P.; Chen, X. M. *Angew. Chem., Int. Ed.* **2006**, *118*, 1587-1589.
- (22) Banerjee, R.; Phan, A.; Wang, B.; Knobler, C.; Furukawa, H.; O'keeffe, M.; Yaghi, O. M. *Science* **2008**, *319*, 939-943.
- (23) Yang, J.; Zhang, F.; Lu, H.; Hong, X.; Jiang, H.; Wu, Y.; Li, Y. *Angew. Chem., Int. Ed.* **2015**, *54*, 10889-10893.
- (24) Ban, Y.; Li, Z.; Li, Y.; Peng, Y.; Jin, H.; Jiao, W.; Guo, A.; Wang, P.; Yang, Q.; Zhong, C.; Yang, W. *Angew. Chem., Int. Ed.* **2015**, *54*, 15703-15707.
- (25) Fan, L.; Liu, P. F.; Yan, X.; Gu, L.; Yang, Z. Z.; Yang, H. G.; Qiu, S.; Yao, X. *Nat. Commun.* **2016**, *7*, 10667.
- (26) Kuhl, K. P.; Hatsukade, T.; Cave, E. R.; Abram, D. N.; Kibsgaard, J.; Jaramillo, T. F. *J. Am. Chem. Soc.* **2014**, *136*, 14107-14113.
- (27) Back, S.; Lim, J.; Kim, N.-Y.; Kim, Y.-H.; Jung, Y. *Chem. Sci.* **2017**, *8*, 1090.
- (28) Lu, Q.; Rosen, J.; Zhou, Y.; Hutchings, G. S.; Kimmel, Y. C.; Chen, J. G.; Jiao, F. *Nat. Commun.* **2014**, *5*, 3242.
- (29) Ma, M.; Trzesniewski, B. J.; Xie, J.; Smith, W. A. *Angew. Chem., Int. Ed.* **2016**, *55*, 9748-9752.

(30) Dunwell, M.; Lu, Q.; Heyes, J. M.; Rosen, J.; Chen, J. G.; Yan, Y.; Jiao, F.; Xu, B. *J. Am. Chem. Soc.* **2017**, *139*, 3774–3783.

1
2
3
4
5
6
7
8
9
10
11
12
13
14
15
16
17
18
19
20
21
22
23
24
25
26
27
28
29
30
31
32
33
34
35
36
37
38
39
40
41
42
43
44
45
46
47
48
49
50
51
52
53
54
55
56
57
58
59
60